JOURNAL OF GEOPHYSICAL RESEARCH, VOL. 90, NO. A10, PAGES 9845–9861, OCTOBER 1, 1985

A Reexamination of Important N_2 Cross Sections by Electron Impact With Application to the Dayglow: The Lyman-Birge-Hopfield Band System and N I (119.99 nm)

J. M. AJELLO

Jet Propulsion Laboratory, California Institute of Technology, Pasadena

D. E. SHEMANSKY

Lunar and Planetary Laboratory, University of Arizona, Tucson

The far ultraviolet emission spectrum (120 to 210 nm) of electron-excited N_2 has been obtained in a crossed-beam laboratory experiment. The cross section of the Lyman-Birge-Hopfield (LBH) band system ($a^1\Pi_g \rightarrow X^1\Sigma_g^+$) has been remeasured using experimental techniques we have previously developed for this metastable transition. The improved laboratory data set for the $a^1\Pi_g$ state allows a determination of the excitation, emission, and predissociation cross section from threshold to 200 eV for use in planetary atmosphere models of the dayglow and aurora. An analytic fit to the experimental cross section allows accurate estimates to arbitrarily high excitation energy. The close agreement in both energy dependence and absolute cross section values between the emission measurements, presented here, and published electron scattering results shows cascade is small (<5%). The total excitation cross section for the N_2 $a^1\Pi_g$ state is estimated to be $6.22 \pm 1.37 \times 10^{-18}$ cm^2 at 100 eV. The absence of emission bands for $v' \geq 7$ suggests the predissociation yield is unity. The excitation function of each vibrational level is found to have the same shape to within 5%. In the low-energy region, $\varepsilon < 20$ eV, differences in excitation threshold lead to a significant departure of the relative vibrational cross sections from the Franck-Condon distribution. Thus the relative LBH vibrational population distribution in a planetary dayglow or aurora is affected by the energy distribution of the electron flux; and we show that atmospheric models need to include this threshold effect. The N I (119.99 nm) cross section has also been remeasured and found to be $3.48 \pm 0.77 \times 10^{-18}$ cm^2 at 200 eV on the basis of a comparison with Lyman α emission from dissociative excitation of H_2.

INTRODUCTION

We present the N_2 electron impact excitation cross sections in the vacuum ultraviolet (VUV) from 40 to 210 nm in a two-part series. From an instrumental point of view the VUV spectrum of N_2 can be conveniently separated into two spectral regions: the extreme ultraviolet (EUV) from 40 to 120 nm and the far ultraviolet (FUV) from 120 to 210 nm. In the EUV region, channeltron detectors (or windowless photomultipliers) are used, and in the FUV, photomultiplier detectors with vacuum-sealed photocathodes. In this paper we concentrate on the FUV region. We show in Figure 1 a calibrated, optically thin electron impact–induced fluorescence spectrum (relative accuracy ~20%) from 50 to 190 nm at 100 eV electron impact energy. Approximately 100 features can be identified at the instrumental resolution of 0.4 nm. Clearly, the EUV is more intense than the FUV. Both regions are rich in atomic lines and molecular features.

In order to model atmospheric UV emissions by N_2 it is necessary to begin the calculation by having at hand a reliable set of laboratory cross section data. To date there has not been a complete study of the entire VUV spectral range with the goal of providing all of the significant cross sections. We provide such a data set at an accuracy of ~20% and identification of all features in Figure 1, beginning with the FUV spectral region.

The Lyman-Birge-Hopfield (LBH) band system is a prominent and important UV emission source in the terrestrial dayglow and aurora. The sole excitation source of the LBH band system is direct electron impact [*Meier et al.*, 1980], and because of this fact it should in principle be a direct monitor of total energy deposition. Rocket and satellite spectra of the FUV region of the dayglow and aurora [*Gentieu et al.*, 1979; *Park et al.*, 1977; *Huffman et al.*, 1980; *Takacs and Feldman*, 1977; *Rottman et al.*, 1973; *Paresce et al.*, 1972] have measured emissions from both atomic nitrogen multiplets and the LBH band system. Additionally, in the outer solar system the LBH band system, many N I and N II atomic multiplets, and several molecular Rydberg systems were detected in the Titan atmosphere by the Voyager ultraviolet spectrometer [*Strobel and Shemansky*, 1982]. Detailed studies show that the radiation from the atomic nitrogen multiplets arises principally from dissociative excitation (earth aurora, Titan dayside emissions) and direct electron excitation of atomic nitrogen (earth dayglow) [*Meier et al.*, 1980; *Park et al.*, 1977].

We have established a laboratory program at the Jet Propulsion Laboratory (JPL) to measure a primary data set consisting of calibrated optically thin VUV fluorescence spectra (40–200 nm) and absolute excitation cross sections (0–0.5 keV) for stable gases which are candidate species for electron impact in the upper atmosphere of the planets and in the atmospheres of cool stars and interstellar molecular clouds. We have made the first steps in this program by completing studies of the singlet states of H_2 [*Ajello et al.*, 1982, 1984; *Shemansky and Ajello*, 1983], the benchmark dissociative cross section of H_2 to produce Lyman α [*Shemansky et al.*, 1985*a*], the atomic emissions of He [*She-*

Paper number 5A8472.
0148-0227/85/005A-8472$05.00

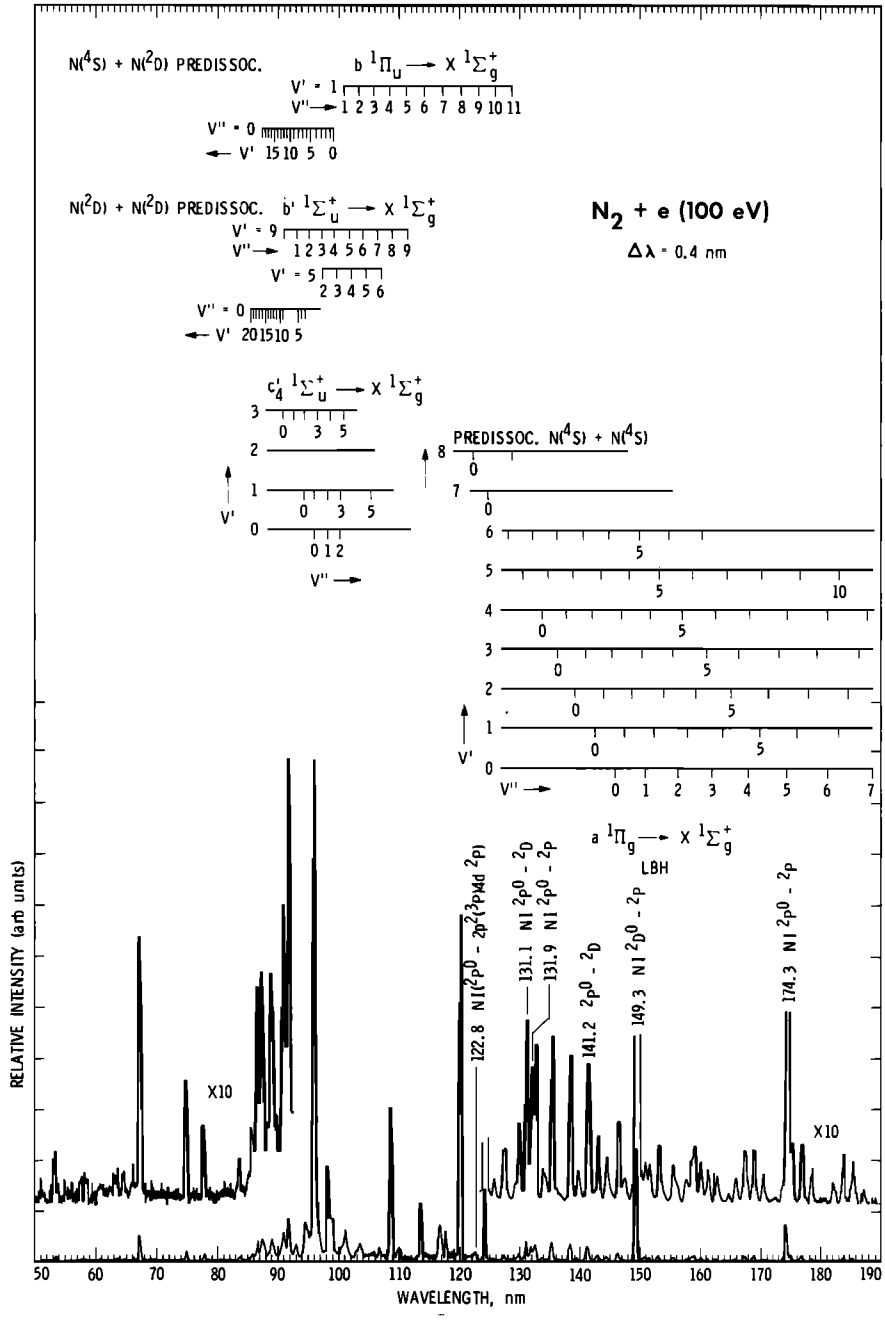

Fig. 1. Calibrated optically thin vacuum ultraviolet spectrum of N_2 at 100 eV electron impact energy at 0.4 nm resolution from 50 to 190 nm. Some of the important Rydberg and LBH vibrational bands are indicated. A few of the FUV N I multiplets are indicated. The spectrum was obtained in the crossed-beam mode. The FUV spectrum was obtained at a background pressure of 1×10^{-5} torr, and the EUV spectrum was obtained at a background pressure of 2×10^{-6} torr. The two spectra were joined at 120.0 nm. The EUV spectral region will be discussed in a future paper.

mansky et al., 1985*b*], and the VUV spectrum of O_2 and H_2O from 40 to 200 nm [*Ajello and Franklin*, 1985; *Ajello*, 1984].

One of us has previously published a laboratory FUV study of N_2 [*Ajello*, 1970] in which experimental problems at electron impact energies above 30 eV seriously compromised the accuracy of the cross-section measurements of the LBH transition and atomic nitrogen multiplets. This problem has already been pointed out in the literature [*Finn and Doering*, 1976]. A problem of backscattering of secondary electrons from the Faraday cup led to an overestimate of cross sections for energies above 30 eV. However, for energies below 30 eV a review of all published LBH cross-section measurements by *Cartwright et al.* [1977*a*, *b*] has shown agreement (~30%) among experimenters. There still remains a need to reexamine the LBH band system and atomic multiplets by optical means with a calibrated electron impact emission spectrometer particularly in the threshold region, 8 to 20 eV. All previous low-energy laboratory studies have been carried out by electron energy loss experiments [*Cartwright et al.*, 1977*a*, *b*; *Finn and Doering*, 1976] or by time of flight measurements [*Borst*, 1972]. A theoretical determination of the LBH excitation cross section has been performed by *Chung and Lin* [1972]. Absolute emission measurements on the LBH band system were made by

Holland [1969] for energies above 100 eV and by *Aarts and de Heer* [1971] for selected LBH bands and atomic nitrogen multiplets for energies above 50 eV. *Mumma and Zipf* [1971*a*] and *Zipf and McLaughlin* [1978] have measured the cross section of many atomic nitrogen multiplets and Rydberg band systems in the EUV and FUV.

We consider the variation in the threshold energy behavior of each vibrational cross section. In all previously published electron impact experiments of the $a^1\Pi_g$ state, both the electron energy loss experiments [*Cartwright et al.*, 1977*a*, *b*; *Finn and Doering*, 1976] and the optical emission experiments [*Ajello*, 1970], the experimenters have assumed in their modeling and data analysis techniques that the threshold difference (~0.2 eV) between the vibrational levels is too small to lead to any departure from the normal Franck-Condon distribution of vibrational cross sections. On the contrary we show that the excitation rates in the low-energy region, $\varepsilon < 20$ eV, differ from the Franck-Condon distribution. The cross section changes rapidly in the low-energy region because of the forbidden nature of the transition.

In this experiment we measure the emission cross section (cascade plus direct excitation) and predissociation cross section for the LBH band system. These results are compared to electron energy loss measurements of the direct excitation cross section. An analytic approximation to the measured cross section demonstrates the extreme simplicity of the collision strengths at energies above the cross-section peak. Cross sections are also obtained for the FUV atomic nitrogen multiplets. The important cross section for N I emission at 119.99 nm is often used to calibrate VUV spectra [*Morgan and Mentall*, 1983], and we discuss the available cross sections in detail for this transition.

EXPERIMENTAL

The experimental apparatus and VUV calibration techniques have been described in detail in earlier publications [*Ajello and Srivastava*, 1981; *Ajello et al.*, 1982, 1984]. In brief the instrument consists of an electron impact emission chamber in tandem with two UV spectrometers. The instrument is automated and interfaced with a computer. A magnetically or electrostatically collimated beam of electrons is crossed with a beam of gas from a capillary array at a background pressure that can be varied from 1×10^{-7} to 3×10^{-4} torr. The background gas pressure for most FUV measurements is 8×10^{-6} torr. This geometry establishes a point emission source (~1 mm^3) collision region. Additionally, a uniform static gas sample can be admitted to the chamber over the same pressure range. This geometry forms a line source collision region (2 cm long × 1 mm in diameter). The crossed-beam arrangement provides high signal to noise for spectral scans, and the static gas mode provides the best geometry for excitation function measurements and for quantitatively studying the LBH band system [*Ajello*, 1970]. Improvements in the electron gun since our earlier papers [*Ajello and Srivastava*, 1981; *Ajello et al.*, 1982] show that the energy scale can now be calibrated to an accuracy of 0.5 eV. The total root-mean-square (rms) uncertainty of the beam energy, including the width of the energy distribution, is less than 1 eV. Improvements in technique [*Ajello and Srivastava*, 1981] have eliminated the aforementioned Faraday cup problem.

The dual-spectrometer instrument, which also represents an improvement over earlier publications, is shown schematically in Figure 2. The experimental configuration is such that both spectrometers can simultaneously view the collision region. Normally, however, the field of view of one of the spectrometers is oriented orthogonal to both the direction of the electron beam and that of molecular beam. The electron gun is mounted on a rotatable table as shown in Figure 2 and allows a measurement of the angular distribution of the radiation field in order to correct the measured cross section for polarization effects. Each spectrometer is an *f*/5.5 optical system. As presently configured, the EUV spectrometer is equipped with a 1200-lines/mm osmium-coated holographic grating and channeltron detector. Similarly, the FUV spectrometer is equipped with a MgF_2/Al grating and EMI Gencom G photomultiplier (115–180 nm) with a CsI photocathode or EMR Photoelectric F photomultiplier (115–300 nm) with a CsTe photocathode, both detectors with MgF_2 windows. The optical system is capable of 0.1 nm resolution. However, for optimum signal to noise it is generally operated at 0.4 to 0.7 nm resolution, which is sufficient for the purpose of resolving most vibrational or multiplet structure in the FUV. Our data analysis techniques [*Ajello et al.*, 1982, 1984] do not require higher resolution in the FUV, i.e., complete resolution of features, for accurately determining cross sections of overlapping features.

In a crossed-beam experiment an excited (N_2 $a^1\Pi_g$) molecule can travel several centimeters before radiating. This physical condition in effect dictates an important design criterion for the chamber: a characteristic length of greater than 10 cm. This requirement was met by providing a 15-cm electron beam in a cylindrical chamber 32.5 cm in diameter. The theory for calculating the fraction of the excited molecules that radiate inside the rectangular (10° × 11.42°) field of view of the spectrometer has been discussed previously [*Ajello*, 1970]. The geometry is nearly identical to the experimental setup of *Ajello* [1970], and the earlier calculations for this geometry apply. *Holland* [1969] has measured the lifetime of the $a^1\Pi_g$ state to be 80 μs. Reanalysis of absorption measurements made earlier by *Shemansky* [1969] shows good agreement with the Holland lifetime. Using this lifetime, we find that the fractional amount of the total radiation field measured in this experiment is 0.72. Additional lifetime measurements were made by *Pilling et al.* [1971], who find $76 < \tau_{v'} < 116$ μs. The difference in the fraction of the radiation field observed between the lifetime results of Holland and those of Pilling et al. is less than 10%.

CALIBRATION

The calibration method has been described previously [*Ajello et al.*, 1982]. The optical system was calibrated on a relative basis from 115 to 210 nm using molecular branching ratios for N_2 as described by *Mumma* [1972] and *Mumma and Zipf* [1971*b*]. In addition we have improved the technique and introduce a valuable redundancy in calibration by making use of a model of the H_2 emission spectrum [*Ajello et al.*, 1984]. The calibration curve for the configuration that included a G photomultiplier has been published previously [*Ajello et al.*, 1982]. The calibration curve for the F photomultiplier is similar at short wavelengths ($\lambda < 160$ nm) and is not shown. The relative accuracy of the technique is 10%. The advantage of including the H_2 bands is to allow the extension of the calibration technique to lower wavelengths than from N_2 alone. An ultimate short-wavelength limit of 80 nm is possible for H_2, whereas for N_2 alone the limit is 127

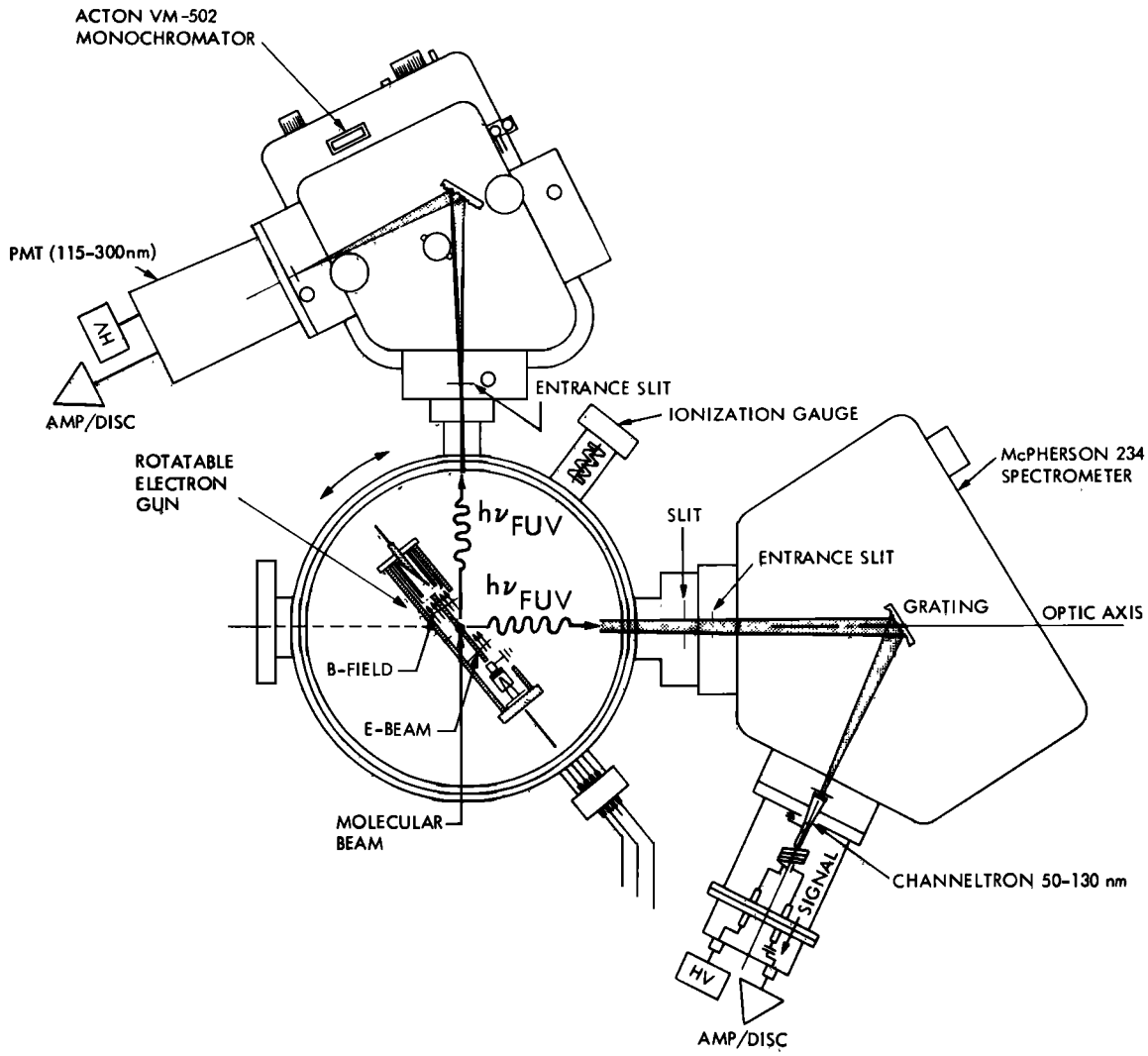

Fig. 2. Schematic diagram of electron impact emission spectrometer with two UV spectrometers: an FUV spectrometer with photomultiplier and an EUV spectrometer with channeltron. The orientation of the electron beam axis is selectable with respect to both optic axes.

nm. At the instrumental resolution of 0.4 nm the N I multiplets are not resolved sufficiently for a branching ratio calibration [*Kelly and Palumbo*, 1973; *Mumma and Zipf*, 1971*a*, *b*]. In summary the LBH bands allow a wavelength calibration from 127 to 260 nm, and the H_2 bands provide a calibration from 80 to 170 nm.

In order to use the LBH system for calibration we provide a set of theoretical calibration factors. These calibration factors, labeled $f_{v'v''}$, are listed in Table 1. The Franck-Condon factors used in the calculation are from *Lofthus and Krupenie* [1977]. The ratios of transition probabilities are taken from *Shemansky* [1969]. We define $f_{v'v''}$ as

$$f_{v'v''} = q_{v'0}\frac{A_{v'v''}}{\Sigma A_{v'v''}} \qquad v' \le 6$$
$$f_{v'v''} = 0 \qquad v' > 6 \tag{1}$$

where $f_{v'v''}$ represents the emission fraction of the total excitation cross section contributed by any molecular band emission. The summation

$$\sum_{\substack{v'=0 \\ \text{all } v''}}^{6} f_{v'v''} = 0.8771$$

since for $v' > 6$ the $a'^1\Pi_g$ state is found in this experiment to be 100% predissociated and bands with $v' > 6$ do not contribute to the emission. We also show that because of threshold effects, (1) is accurate for relative intensity measurements for energies only above ~20 eV. This deviation from (1) does not represent a violation of the Born approximation.

One additional calibration procedure must be considered. The absolute cross section of N I (119.99 nm), used to normalize the entire FUV spectrum, is determined by the relative flow technique developed at JPL [*Srivastava et al.*, 1975; *Trajmar and Register*, 1984]. In this method the Lyman α fluorescence signal from H_2, the standard gas, is compared to the fluorescence signal from N I (119.99 nm) produced by electron impact of N_2, the unknown gas. These comparisons are performed over a range of background gas pressures from 5×10^{-7} to 1×10^{-5} torr to establish linearity

TABLE 1. LBH Relative Cross Sections

Band ($v'v''$)	Wavelength, nm	Theoretical Emission Fraction of Excitation Cross Section $f_{v'v''}$
(0, 0)	145.0	0.24732E−02
(0, 1)	150.1	0.78524E−02
(0, 2)	155.5	0.11490E−01
(0, 3)	161.2	0.10294E−01
(0, 4)	167.2	0.63432E−02
(0, 5)	173.6	0.28342E−02
(0, 6)	180.5	0.95700E−03
(0, 7)	187.8	0.24539E−03
(0, 8)	195.6	0.49077E−04
(0, 9)	204.0	0.61346E−04
(1, 0)	141.6	0.19461E−01
(1, 1)	146.4	0.29275E−01
(1, 2)	151.5	0.10867E−01
(1, 3)	157.0	0.66877E−04
(1, 4)	162.7	0.98643E−02
(1, 5)	168.8	0.18274E−01
(1, 6)	175.2	0.15181E−01
(1, 7)	182.1	0.77911E−02
(1, 8)	189.5	0.27921E−02
(1, 9)	197.3	0.71892E−03
(1, 10)	205.7	0.13375E−03
(1, 11)	214.7	0.16720E−04
(2, 0)	138.4	0.46412E−01
(2, 1)	143.0	0.23809E−01
(2, 2)	147.9	0.75344E−03
(2, 3)	153.0	0.21498E−01
(2, 4)	158.5	0.15068E−01
(2, 5)	164.2	0.75344E−04
(2, 6)	170.3	0.97947E−02
(2, 7)	176.8	0.21247E−01
(2, 8)	183.8	0.18057E−01
(2. 9)	191.1	0.90413E−02
(2, 10)	199.0	0.30389E−02
(2, 11)	207.4	0.75344E−03
(2, 12)	216.5	0.12557E−03
(2, 13)	226.2	0.25115E−04
(3, 0)	135.4	0.58315E−01
(3, 1)	139.8	0.35384E−02
(3, 2)	144.4	0.19694E−01
(3, 3)	149.3	0.16046E−01
(3, 4)	154.5	0.87774E−03
(3, 5)	160.0	0.18241E−01
(3, 6)	165.8	0.10697E−01
(3, 7)	171.9	0.82284E−04
(3, 8)	178.5	0.11438E−01
(3, 9)	185.4	0.19859E−01
(3, 10)	192.8	0.14839E−01
(3, 11)	200.7	0.66379E−02
(3, 12)	209.2	0.20024E−02
(3, 13)	218.2	0.43887E−03
(3, 14)	227.9	0.54859E−04
(4, 0)	132.5	0.48539E−01
(4, 1)	136.8	0.17082E−02
(4, 2)	141.2	0.23916E−01
(4, 3)	145.9	0.97615E−04
(4, 4)	150.8	0.15789E−01
(4, 5)	156.0	0.64426E−02
(4, 6)	161.6	0.30993E−02
(4, 7)	167.4	0.14227E−01
(4, 8)	173.6	0.42707E−02
(4, 9)	180.1	0.14398E−02
(4, 10)	187.1	0.11958E−01
(4, 11)	194.5	0.15033E−01
(4, 12)	202.5	0.91758E−02
(4, 13)	210.9	0.33897E−02
(4, 14)	220.0	0.90294E−03
(4, 15)	229.7	0.17083E−03
(4, 16)	240.2	0.24404E−04
(5, 0)	129.9	0.30414E−01
(5, 1)	133.9	0.10572E−01
(5, 2)	138.2	0.95717E−02
(5, 3)	142.7	0.64001E−02
(5, 4)	147.4	0.93641E−02
(5, 5)	152.3	0.14159E−02
(5, 6)	157.6	0.10742E−01
(5, 7)	163.1	0.77405E−03
(5, 8)	169.0	0.56071E−02
(5, 9)	175.2	0.81558E−02
(5, 10)	181.8	0.45310E−03
(5, 11)	188.8	0.36248E−02
(5, 12)	196.3	0.10119E−01
(5, 13)	204.2	0.90053E−02
(5, 14)	212.7	0.43610E−02
(5, 15)	221.8	0.13593E−02
(5, 16)	231.5	0.30207E−03
(5, 17)	242.0	0.37758E−04
(6, 0)	127.3	0.15369E−01
(6, 1)	131.2	0.14240E−01
(6, 2)	135.3	0.69560E−03
(6, 3)	139.6	0.10053E−01
(6, 4)	144.1	0.31499E−03
(6, 5)	148.9	0.72185E−02
(6, 6)	153.9	0.13518E−02
(6, 7)	159.2	0.39505E−02
(6, 8)	164.8	0.43312E−02
(6, 9)	170.7	0.26249E−03
(6, 10)	176.9	0.54205E−02
(6, 11)	183.5	0.27299E−02
(6, 12)	190.6	0.21000E−03
(6, 13)	198.1	0.45805E−02
(6, 14)	206.0	0.66017E−02
(6, 15)	214.5	0.42393E−02
(6, 16)	223.6	0.16275E−02
(6, 17)	233.3	0.40687E−03
(6, 18)	243.8	0.65623E−04
(6, 19)	255.0	0.13125E−04
Summary total		q_{00} = 0.04308 q_{10} = 0.1155 q_{20} = 0.1707 q_{30} = 0.1832 q_{40} = 0.1600 q_{50} = 0.1217 q_{60} = 0.08296

$$\sum_{\substack{v'=0\\ \text{all } v'}}^{6} f_{v'v''} = \sum_{v'=0}^{6} q_{v'0} = 0.8771$$

Values are at the high-energy limit. Read 0.24732E–02 as 0.24732×10^{-2}.

of signal with pressure. For the comparison of the signal strengths in the linear region a value of 5.78×10^{-18} cm^2 was used for the Lyman α cross section from H_2 at 200 eV [*Shemansky et al.*, 1985*a*]. The cross section for Lyman α production by dissociative excitation is 31% smaller than the value previously found by *Mumma and Zipf* [1971*c*]. *Shemansky et al.* [1985*a*] have revised the Lyman α cross section on the basis of cross-section measurements of the H_2 Lyman and Werner bands and previously measured Lyman α/Lyman band and Lyman α/Werner band electron cross-section ratios [*Ajello et al.*, 1984]. The value of 5.78×10^{-18} cm^2 at 200 eV reflected in these new measurements was used in the relative flow calibration.

Our results show the H_2 (Lyman α)/N_2 (119.99 nm) ratio is 1.66 ± 0.10 at 200 eV; and hence the cross section at 200 eV for production of N I (119.99 nm) is $3.48 \pm 0.37 \times 10^{-18}$ cm^2. The root sum square 1σ uncertainty is 16% determined by the following: (1) 15% uncertainty in the Lyman α standard cross section at 200 eV, (2) 2% uncertainty in the relative Ly

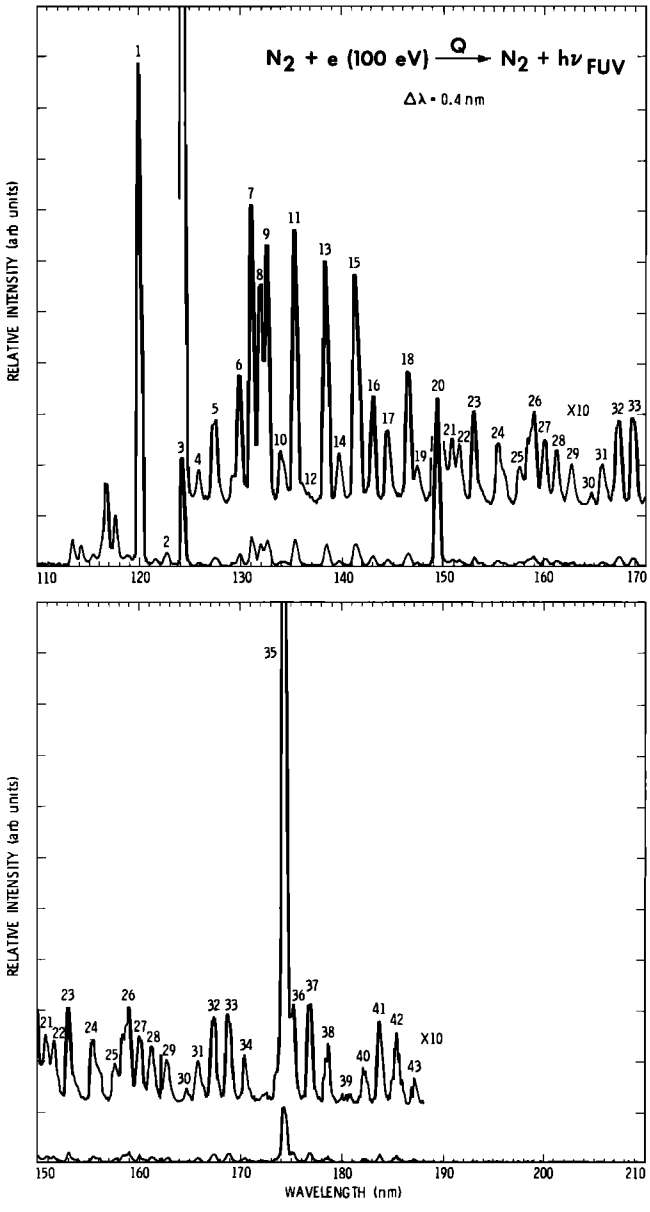

Fig. 3. Calibrated FUV spectrum of N_2 at 100 eV at 0.4 nm resolution with the G photomultiplier. The feature numbers are listed in Table 2 with identification and cross sections. Seventy-two percent of the LBH band system emission is observed.

α/119.99-nm sensitivity calibration, and (3) 5% uncertainty in the signal statistics and repeatability.

In addition, for normalization of the N_2 100-eV spectrum, to be analyzed in the next section, we find the 100-eV cross section of N I (119.99 nm) to be 4.48×10^{-18} cm^2. This value is determined from our excitation function measurements of the next section. The 100-eV to 200-eV cross-section ratio for production of N I (119.99 nm) is 1.29 ± 0.05. However, our absolute cross-section value at 100 eV is 33% below the 6.70×10^{-18} value of *Mumma and Zipf* [1971*a*]. Most of the change (31%) is due to the revised cross-section value of Lyman α; and 2% of the change is due to a slightly larger H_2 (Lyman α)/N_2 (119.99 nm) ratio measured here. Thus one immediate result of our H_2 and N_2 studies is that most cross sections measured over the last decade must be revised downward by 31% if based on Lyman α or 33% if based on N I (119.99 nm) as a calibration standard. *Shemansky et al.* [1985*a*] discuss the implications of these new measurements.

The estimated uncertainties in the LBH cross section and in the N I multiplets, other than for N I (119.99 nm), are 22% and 20%, respectively, determined by the following: (1) 16% uncertainty in the N I cross section, (2) 10% uncertainty in the relative wavelength calibration, (3) 5% uncertainty in the signal statistics and repeatability, and (4) 10% uncertainty in the LBH fraction observed.

RESULTS

We present in this section FUV spectra at 11, 15, 50, and 100 eV and excitation function measurements from 0 to 200 eV. Comparison of present results to published data shows that a reliable set of cross sections now exists for the FUV spectral region. In addition, threshold effects that appear to have been overlooked in the literature are examined in detail.

Spectra of N_2 at 100 eV and 50 eV are shown in Figures 3 and 4, obtained with the G photomultiplier and F photomultiplier detectors, respectively. Spectra of N_2 at 15 and 11 eV with the F photomultiplier are given in Figure 5. Figures 4 and 5 contain models of the spectral data. A detailed analysis of the observed 54-LBH and N I features at 100 eV excitation energy, between 120 and 210 nm, is given in Table 2. The N_2 LBH band emission features represent 85.8% of the electronic excitation cross section for the $a^1\Pi_g$ state and extend ultimately to 260 nm. The electronic emission cross section is 87.71% of the excitation cross section for the $a^1\Pi_g$ state. The predissociation cross section accounts for the remaining 12.29% of the electronic excitation cross section. Included with the list of observed band features in Table 2 are the cross sections at 100 eV for each LBH feature. Cross sections at 100 and 200 eV are also given for the N I multiplets [*Kelly and Palumbo*, 1973; *Wiese et al.*, 1966] in Table 2. A total electron cross section for the $a^1\Pi_g$ state corrected for the unobserved 1.94% of the band system is given at the end of Table 2. We find for the $a^1\Pi_g$ state at 100 eV that $Q_E = 5.46 \times 10^{-18}$ cm^2, $Q_P = 0.76 \times 10^{-18}$ cm^2, and $Q = 6.22 \times 10^{-18}$ cm^2 where Q is the excitation cross section, Q_E is the emission cross section, and Q_P is the predissociation cross section at energy ε. The three cross sections are related by

$$Q = Q_E + Q_P \tag{2}$$

Q_E is the sum of cascade and direct excitation cross sections. Our results indicate that the cascade contribution is negligible (<5%). We will discuss this point again.

The LBH cross section can be measured in two ways, through summation of the contributions of all bands, or by measurement of the emission cross section of any strong band, and translating to the total cross section using the $f_{v'v}$ values of Table 1. The results from the two methods in this experiment using the (3, 0) band agree to 2.5%. For consistency we give (Table 2) average cross-section values for each band within the 22% uncertainty based on the total measured cross section of 6.22×10^{-18} cm^2 at 100 eV.

Equally important cross-section values were obtained for the N I multiplets. We show in Table 3 the experimental results for the N I lines at 100 eV. The cross sections of several of the multiplets, determined by the branching ratio technique described by *Mumma and Zipf* [1971*a*], are compiled in Table 3. As explained previously, we find most of our results tend to be about 30% below those of Mumma and Zipf. An exception occurs for the weak 116.40- and 131.07-

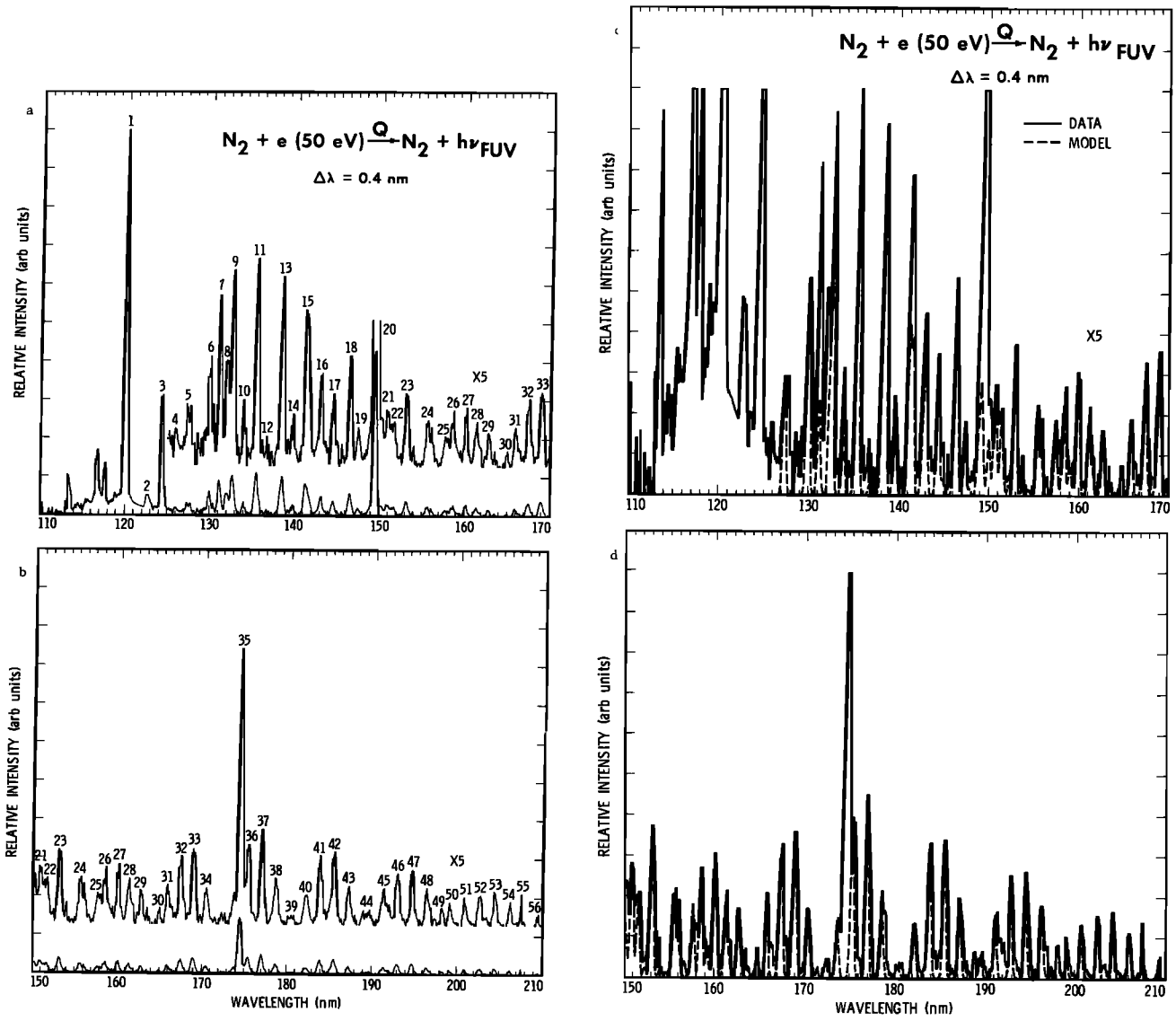

Fig. 4. (*a* and *b*) Calibrated FUV spectrum of N_2 at 50 eV with 0.4 nm resolution using the F photomultiplier. (*c* and *d*) Overplot of laboratory spectrum (× 5) and synthetic spectrum at 0.4 nm resolution. The model assumes a Gaussian monochromator slit function with no rotational structure.

nm multiplets. The original results of Mumma and Zipf for the 116.40-nm multiplet may be too high by about a factor of 2 because their measurement probably contains other N I multiplet contributions [*Kelly and Palumbo*, 1973].

Excitation functions of the (3, 0) LBH band at 135.37 nm and of the N I (119.99 nm) multiplet have been obtained and tabulated in Tables 4, 5, and 6. Table 4 lists the relative LBH cross-section energy dependence from threshold to 200 eV for the (3, 0) band from the experimental data and for a model based on the (3, 0) data. The model described in the following section allows analytic calculation of the excitation function. Table 5 contains the calculated absolute LBH excitation cross section (emission plus predissociation) from threshold to 200 eV based on the analytic excitation function. Table 6 lists the N I (119.99 nm) dissociative cross section from threshold to 400 eV. In addition the same information is shown graphically. We show plots of the energy dependence of the cross sections in Figures 6, 7, 8, and 9. Figure 6 shows the experimentally measured (3, 0) cross section from threshold to 200 eV. Figure 7 shows the N I (119.99 nm) dissociative cross section from threshold to 200 eV. Figure 8 shows both cross sections from threshold to 50 eV and a model of the (3, 0) band. Figure 9 plots the modeled relative cross sections for each N_2 $a^1\Pi_g$ vibrational level in the threshold region. Most of the discussion that follows, particularly of the threshold effect, requires an introduction into the nature of the LBH cross-section model and an understanding of the distinctive shape function of the collision strength.

Analytic Approximation of the N_2 LBH Cross Section

A method of establishing excitation cross sections using analytic approximations has been recently applied to electron excitation of H_2 and He allowed transitions [*Shemansky et al.*, 1985*a*, *b*]. The method provides the means of establishing absolute cross sections for allowed transitions, and in addition gives an indication of the role played by exchange and configuration mixing effects in the excitation process. We find in the case of the N_2 LBH excitation function that

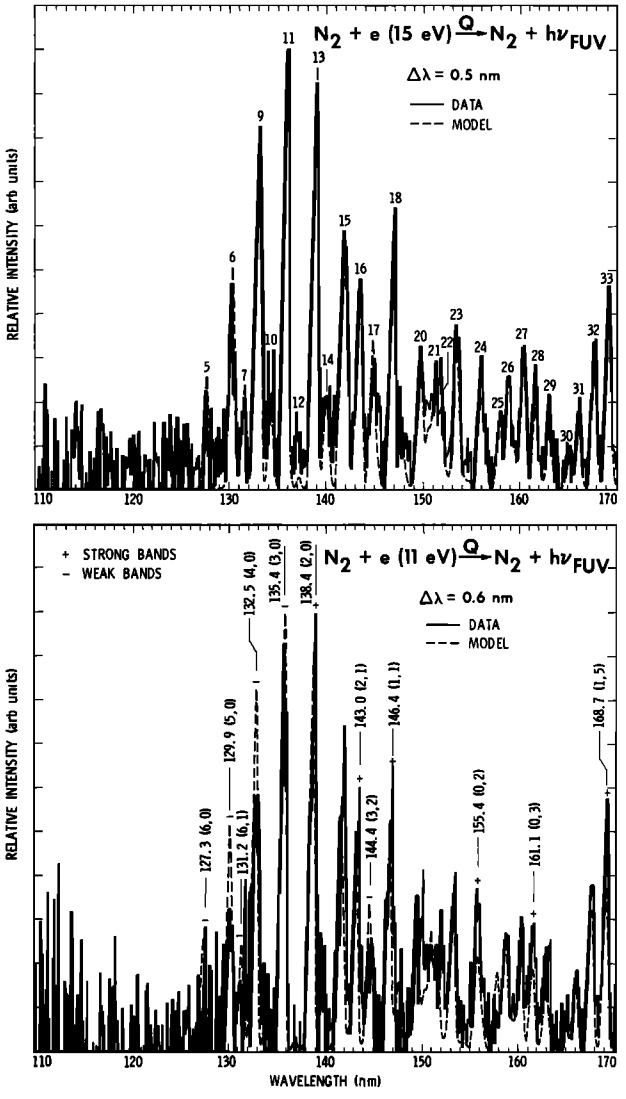

Fig. 5. Calibrated FUV spectra of N_2 at (top) 15 eV at 0.5 nm resolution and (bottom) 11 eV at 0.6 nm resolution using the F photomultiplier. Both plots are based on the assumption of Franck-Condon distribution of relative vibrational cross sections. In the model the (3, 0) band is the strongest band, and in all the spectral data for $\varepsilon \geq 15$ eV the strongest band is the (3, 0) band. The data and model are normalized together at the (3, 0) band for the 15-eV spectrum. Bands that have increased in intensity (hence emission cross section) at 11 eV in relation to the (3, 0) band are called strong bands ($v' > 3$), and bands that have decreased in intensity ($v' < 3$) are called weak bands in the bottom panel.

the analytic form used by *Shemansky et al.* [1985*b*] cannot be applied because of the extremely sharp transition region of the collision strength near threshold. The measured excitation function of the N_2 LBH bands has been fitted with an analytic function, using a collision strength Ω_{ij} of the form

$$\Omega_{ij}(X) = C_{ij}\{1 - \exp[7 \ln X - \alpha(X - 1)]\} \quad (3)$$

where $X = \varepsilon/E_{ij}$, $\alpha = 7.1675$, ε is electron energy, E_{ij} is the excitation threshold energy, and C_{ij} is a constant. The cross section Q_{ij} is given by

$$Q_{ij}(\varepsilon) = \frac{\Omega_{ij}}{\omega_i}\frac{1}{\varepsilon} \text{ au} \quad (4)$$

where $\omega_i = 1$ is lower state degeneracy, and ε is in Rydberg units.

The form of (3) differs substantially from the analytic expressions used to fit excitation functions of most other transitions [see *Shemansky et al.*, 1985*b*]. In this sense the basic characteristic that separates the N_2 LBH collision strength shape from other electron exchange–dominated excitation transitions is a very rapid rise from threshold to a constant value. The collision strength is virtually constant for $X > 2$, as shown in Figure 10. Equation (3) fits the observed curve to 5% with the exception of the values at 10 and 12 eV (Table 4). However, the low-energy deviation may be caused largely by the finite energy width of the experimental electron beam.

The simplicity and accuracy of the fit of (3) and (4) to the observed data, with a very rapid transition to a constant collision strength characteristic of an exchange transition, suggest that the emission is unaffected by cascade from higher states. The constancy of Ω_{ij} for $X > 2$ (Figure 10) allows accurate calculation of cross sections at energies beyond the upper limit of the experimental measurement. We discuss below the importance of applying (3) and (4) separately for each vibrational level because of differences in E_{ij} values. Tables 4 and 5 and Figure 8 show the calculated cross sections compared to measurement. Table 5 lists values of C_{ij} and E_{ij} for each vibrational level, allowing accurate calculation of cross sections at any energy using (3) and (4). Additionally, Table 5 lists $Q_{v'}$, the vibrational excitation cross section at 100 eV, for normalizing the vibrational cross sections and verifying calculations based on (3) and (4).

The nature and magnitude of threshold effects are discussed in the following section.

Threshold Effects in the N_2 ($a^1\Pi_g \rightarrow X^1\Sigma_g^+$) Cross Section

The excitation function of each LBH band feature is the same to within the experimental accuracy (~5% for the stronger bands, e.g., (3, 0), (2, 0), (1, 1)) apart from differences in threshold energy. The constant α in (3) is therefore the same value for each $a^1\Pi_g$ vibrational level. The $v' = 0$ threshold is at 8.55 eV; the $v' = 3$ threshold is at 9.16 eV; and the $v' = 6$ threshold is at 9.75 eV. Thus the cross-section energy dependence of each vibrational level is displaced about 0.20 eV from the adjacent vibrational level. Although this energy difference between vibrational levels is small, it has important implications in the low-energy region ($\varepsilon < 20$ eV) where the cross section is changing rapidly with energy.

Table 4 gives the measured relative cross section for the $a^1\Pi_g$ (3, 0) band and compares the experimental result to other measurements and analytic calculations of the $a^1\Pi_g$ electronic cross section. Figure 8 shows a plot of the experimental data and model for the (3, 0) band. In this comparison it is seen that the relative variation of the $v' = 3$ vibrational level cross section is the same as the modeled variation to within 5% except at 12 eV and 10 eV, where deviations are 17% and 10%, respectively. A substantial part of these deviations are probably caused by the finite energy width of the electron beam as noted above. Both the data and the model for the (3, 0) band fall off more rapidly with respect to decreasing energy below the peak than do the other experimental data in Table 4. Previous analysis of the excitation cross section has assumed applicability of the Franck-Condon distribution of vibrational cross sections down to threshold. This assumption would tend to overestimate total cross sections in the threshold energy region.

TABLE 2. Features of Far Ultraviolet Spectrum of N_2 at 100 eV

Feature	Band, nm, Theory	Peak or Head, nm, Observed	Identification	$f_{v'v''}$	Q_E (10^{-19} cm^2), 100 eV	Q_{LBH} (10^{-19} cm^2), 100 eV	Q_{NI} (10^{-19} cm^2), 100 eV (200 eV)
1	N I 119.99ST	120.0	g^4S^0–^4P		44.8		44.8
	N I 120.02ST		g^4S^0–^4P				(34.8)
	N I 120.07ST		g^4S^0–^4P				
2	N I 122.50	122.7	$^2P^0$–^2D		3.06		
	N I 122.54		$^2P^0$–^2D				
	N_2 122.66		a (8, 0)				
	N_2 122.67		b (1, 9)				
	N I 122.84		$^2P^0$–^2P				
	N I 122.88		$^2P^0$–^2P				
	N I 123.05		$^2P^0$–^2P				
3	N I 124.33	124.3	$^2D^0$–^2D		11.3		11.3
							(8.80)
4	N_2 125.87	126.0	b (1, 10)		0.66		
	N_2 126.29		a (8, 1)				
5	N_2 127.32	127.4	a (6, 0)	0.1537E−01	0.95	0.95	
	N II 127.50P		$^3D^0$–^3P				
	N II 127.53P		$^3D^0$–^3P				
	N II 127.62P		$^3D^0$–^3P				
	N II 127.68P		$^3D^0$–^3P				
6	N_2 129.85	129.8	a (5, 0)	0.3041E−01	1.88	1.88	
7	N I 131.07	131.1	$^2P^0$–^2D		3.25		2.37
	N_2 131.2		a (6, 1)	0.1424E−01		0.88	(1.83)
8	N I 131.95	131.9	$^2P^0$–^2P		1.86		1.86
							(1.60)
9	N_2 132.53	132.5	a (4, 0)	0.4854E−01	3.60	3.01	
	N I 132.70		$^2P^0$–^2P				0.59
							(0.47)
10	N_2 133.90		a (5, 1)	0.1057E−01	0.65	0.65	
11	N_2 135.2	135.3	a (6, 2)	0.6956E−03	3.66	0.043	
	N_2 135.37		a (3, 0)	0.5832E−01		3.62	
12	N_2 136.7	136.7	a (4, 1)	0.1708E−02	0.11	0.11	
13	N_2 138.16	138.3	a (5, 2)	0.9572E−02	3.46	0.59	
	N_2 138.38		a (2, 0)	0.4641E−01		2.87	
14	N_2 139.59	139.6	a (6, 3)	0.1005E−01	0.84	0.62	
	N_2 139.8		a (3, 1)	0.3538E−02		0.22	
15	N_2 141.19	141.2	a (4, 2)	0.2392E−01	3.93	1.48	
	N_2 141.59		a (1, 0)	0.1946E−01		1.21	
	N I 141.19		$^2P^0$–^2D				1.24
16	N_2 142.63	143.0	a (5, 3)	0.6400E−02	1.84	0.39	
	N_2 142.99		a (2, 1)	0.2381E−01		1.45	
17	N_2 144.0	144.4	a (6, 4)	0.3149E−03	1.39	0.02	
	N_2 144.42		a (3, 2)	0.1969E−01		1.21	
	N_2 145.01		a (0, 0)	0.2472E−02		0.16	
18	N_2 145.9	146.4	a (4, 3)	0.9761E−04	1.83	0.006	
	N_2 146.4		a (1, 1)	0.2928E−01		1.82	
19	N_2 147.35	147.3	a (5, 4)	0.9364E−01	0.62	0.59	
	N_2 147.9		a (2, 2)	0.7534E−03		0.13	
20	N_2 148.8	149.3	a (6, 5)	0.7219E−02	18.7	0.45	
	N_2 149.3		a (3, 3)	0.1605E−01		1.00	
	N I 149.33		$^2D^0$–^2P				16.8
	N_2 150.1		(0, 1)	0.7852E−02		0.49	(13.1)
21	N_2 150.81	150.7	a (4, 4)	0.1579E−01	0.95	0.98	
22	N_2 151.53	151.5	a (1, 2)	0.1087E−01	0.76	0.68	
	N_2 152.3		a (5, 5)	0.1416E−02		0.08	
23	N_2 153.0	153.0	a (2, 3)	0.2150E−01	1.46	1.33	
	N_2 153.8		a (6, 6)	0.1352E−02		0.08	
	N_2 154.5		a (3, 4)	0.8777E−03		0.054	
24	N_2 155.45	155.4	a (0, 2)	0.1149E−01	1.09	0.70	
	N_2 156.02		(4, 5)	0.6443E−02		0.39	
25	N_2 157.0	157.5	a (1, 3)	0.6688E−04	0.66	0.0041	
	N_2 157.5		a (5, 6)	0.1074E−01		0.66	
26	N_2 158.44	158.8	a (2, 4)	0.1501E−01	1.17	0.93	
	N_2 159.15		a (6, 7)	0.3951E−02		0.24	
27	N_2 159.97	159.9	a (3, 5)	0.1824E−01	1.13	1.13	
28	N_2 161.14	161.1	a (0, 3)	0.1029E−01	0.84	0.64	
	N_2 161.53		a (4, 6)	0.3099E−02		0.20	
29	N_2 162.66	162.6	a (1, 4)	0.9864E−02	0.66	0.61	
	N_2 163.11		a (5, 7)	0.7741E−03		0.048	
30	N_2 164.73	164.6	a (6, 8)	0.4331E−02	0.28	0.28	
31	N_2 165.76	165.8	a (3, 6)	0.1070E−01	0.66	0.66	
32	N_2 167.19	167.3	a (0, 4)	0.6343E−02	1.26	0.38	
	N_2 167.36		a (4, 7)	0.1423E−01		0.88	

TABLE 2. (continued)

Feature	Band, nm, Theory	Peak or Head, nm, Observed	Identification	$f_{v'v''}$	Q_E (10^{-19} cm^2), 100 eV	Q_{LBH} (10^{-19} cm^2), 100 eV	Q_{NI} (10^{-19} cm^2), 100 eV (200 eV)
33	N_2 168.74	168.7	*a* (1, 5)	0.1827E−01	1.48	1.13	
	N_2 168.98		*a* (5, 8)	0.5607E−02		0.35	
34	N_2 170.31	170.3	*a* (2, 6)	0.9795E−02	0.63	0.61	
	N_2 170.5		*a* (6, 9)	0.2625E−03		0.016	
35	N_2 173.54	174.2	*a* (4, 8)	0.4271E−02	6.94	0.26	
	N_2 173.61		*a* (0, 5)	0.2834E−02		0.18	
	N I 174.36		$^2P^0$–^2P				6.51 (5.06)
36	N_2 175.19	175.1	*a* (5, 9)	0.8156E−02	1.45	0.51	
	N_2 175.20		*a* (1, 6)	0.1518E−01		0.94	
37	N_2 176.81	176.7	*a* (2, 7)	0.2125E−01	1.66	1.32	
	N_2 176.82		*a* (6, 10)	0.5421E−02		0.34	
38	N_2 178.44	178.5	*a* (3, 5)	0.1824E−01	1.13	1.13	
39	N_2 180.10	180.4	*a* (4, 9)	0.1440E−02	0.14	0.08	
	N_2 180.46		*a* (0, 6)	0.9570E−03		0.06	
40	N_2 182.08	182.2	*a* (1, 7)	0.7791E−02	0.49	0.49	
41	N_2 183.50	183.7	*a* (6, 11)	0.2730E−02	1.30	0.18	
	N_2 183.72		*a* (2, 8)	0.1806E−01		1.12	
42	N_2 185.38	185.4	*a* (3, 9)	0.1986E−01	1.23	1.23	
43	N_2 187.08	187.1	*a* (4, 10)	0.1196E−01	0.74	0.74	
44	N_2 189.42	189.4	*a* (1, 8)	0.2792E−02	0.18	0.18	
45	N_2 191.09	191.2	*a* (2, 9)	0.9041E−02	0.56	0.56	
46	N_2 192.78	192.8	*a* (3, 10)	0.1484E−01	0.92	0.92	
47	N_2 194.50	194.7	*a* (4, 11)	0.1503E−01	0.94	0.94	
	N_2 195.59		*a* (0, 8)	0.4908E−04		0.003	
48	N_2 196.24	196.3	*a* (5, 12)	0.1012E−01	0.63	0.63	
49	N_2 198.01	198.1	*a* (6, 13)	0.4581E−02	0.28	0.28	
50	N_2 198.96	199.0	*a* (2, 10)	0.3039E−02	0.19	0.19	
51	N_2 200.6	200.8	*a* (3, 11)	0.6638E−02	0.41	0.41	
52	N_2 202.35	202.4	*a* (4, 12)	0.9176E−02	0.70	0.70	
53	N_2 204.12	204.3	*a* (5, 12)	0.1012E−01	0.63	0.63	
54	N_2 205.90	205.9	*a* (6, 14)	0.6602E−02	0.41	0.41	
Totals				0.8577*		$Q_E = 5.46 \times 10^{-18}$ cm^2†	
						$Q_P = 0.76 \times 10^{-18}$ cm^2	
						$Q = 6.22 \times 10^{-18}$ cm^2	

ST and P follow notation of *Kelly and Palumbo* [1973]. ST is Standard Line, and P is predicted wavelength.

*85.77% of possible band system emission of 87.71% observed by F photomultiplier tube; also 76.6% of band system emission observed by G photomultiplier tube.

†Represents total emission cross section including 1.94% of emission from region between 205.9 and 260.0 nm.

TABLE 3. Excitation Cross Sections of the N I Multiplets in the FUV at 100 eV by Dissociative Excitation

Wavelength, nm	Transition	Cross Sections,* 10^{-18} cm^2	Data From *Aarts and de Heer* [1971]	Data From *Mumma and Zipf* [1971*a*]	Data From *Ajello* [1970]
116.40†	$^2D^0$–^2D	0.08	0.62	0.163	
117.69‡	$^2D^0$–^2P	0.33	0.44	0.516	
119.99	$^4S^0$–^4P	4.48	4.72	6.7	7.4
124.33§	$^2D^0$–^2D	1.13	1.52	1.45	
131.07†	$^2P^0$–^2D	0.23		0.452	
131.95	$^2P^0$–^2P	0.19			
132.70	$^2P^0$–^2P	0.06		0.093	
141.19§	$^2P^0$–^2D	0.12		0.16	
149.33	$^2D^0$–^2P	1.68	1.88	2.53	5.7
174.36	$^2P^0$–^2P	0.65	0.77	0.91	2.1

*Contributions from LBH bands have been subtracted.

†The 116.40/131.07 cross-section ratio is given by the branching ratio of 0.36/1 [see *Mumma and Zipf*, 1971*a*]. The 131.07-nm cross section was measured; see Table 2.

‡The 117.69/132.70 cross-section ratio is in the branching ratio of 5.5/1 [see *Mumma and Zipf*, 1971*a*]. The 117.69-nm cross section was measured and will be discussed in a forthcoming EUV paper.

§The 124.33/141.19 cross-section ratio is in the branching ratio of 9.1/1 [see *Mumma and Zipf*, 1971*a*]. The 124.33-nm cross section was measured; see Table 2.

TABLE 4. Relative Cross Section of N_2 ($a^1\Pi_g \rightarrow X^1\Sigma_g^+$) by Electron Impact

	Relative Cross Section								
Energy, eV	(3,0) Band Observed Data, This Work	(3, 0) Band Analytic Fit to Observed Data*	Normalized Total $a^1\Pi_g$ Cross Section Q, This Work	Q_E From *Holland* [1969]	Q_E From *Aarts and de Heer* 1971]	Q From *Cartwright et al.* [1977*b*]	Q_E From *Borst* [1972]	Q From *Chung and Lin* [1972]	Q From *Finn and Doering* [1976]
9.16 (A.P)	0					0			
10	0.094	0.086	0.082			0.20	0.24		
12	0.41	0.48	0.45			0.40	0.55		
14	0.81	0.81	0.79			0.73	0.91		
16	0.98	0.97	0.96			0.95	1.00	1.00	1.00
17	1.0	1.0	0.99			1.00	0.93		1.00
18	0.99	1.0	1.00			0.95	0.91		1.00
20	0.94	0.96	0.97			0.91	0.74	0.91	0.86
25	0.79	0.81	0.82			0.78	0.63	0.64	
30	0.68	0.67	0.69			0.68	0.52		0.64
35	0.58	0.58	0.59			0.60	0.46	0.50	0.47
40	0.51	0.51	0.52			0.53		0.40	0.42
50	0.40	0.40	0.41			0.42		0.36	0.28
60	0.35	0.34	0.34		0.35†			0.36	0.22
70	0.29	0.29	0.30						
80	0.26	0.26	0.26		0.27			0.26	
90	0.23	0.22	0.23						0.16
100	0.20	0.20	0.21	0.20†	0.23			0.19	0.14
150	0.14	0.13	0.14		0.18				
200	0.11	0.10	0.10	0.11	0.14			0.11	

A.P. is appearance potential.
*See text.
†Normalized to result of this work at the same energy.

The total N_2 $a^1\Pi_g$ cross section as well as Q_E and Q_P, calculated using the analytic function (equations (3) and (4)), are given in Table 5. The values of Q_E and Q_P given in Table 5 for energies $\varepsilon \geq 20$ eV agree with the Franck-Condon ratios for these quantities to better than 5%. The modeled energy dependence of each vibrational level is shown in Figure 9. In the energy region from the $v' = 0$ threshold at 8.55 eV to 20 eV, we must rely on a detailed model of the threshold energy behavior of each vibrational level to determine the energy dependence of the total cross section. At higher energies, $\varepsilon \geq 20$ eV, the relative $a^1\Pi_g$ vibrational excitation rates gradually converge on the Franck-Condon distribution. Figure 9 demonstrates the variation in the ratio of the vibrational cross sections with energy in the threshold energy region, $\varepsilon < 20$ eV. For example, above 12.5 eV the $v' = 3$ level has the largest vibrational cross section. Below 12.5 eV the $v' = 2$ level has the largest cross section. At

TABLE 5*a*. Total Excitation, Emission, and Predissociation Cross Section for N_2 ($a^1\Pi_g \rightarrow X^1\Sigma_g^+$)

ε, Energy	Q*	Q_E*	Q_P*	Q†	Q‡	Q_E§	Q‖	Q_E¶
10	2.46	2.45	0.01	5.9				
12	13.6	12.8	0.8	14.0				
14	23.6	21.6	2.08	22.0				
16	28.8	25.9	2.96	28.6				38.5
17	29.9	26.7	3.21	30.2	36			
18	30.2	26.8	3.36	29.7				
20	29.3	25.9	3.43	27.6	31			
25	24.7	21.7	3.04	23.5				
30	20.7	18.2	2.57	20.4	23			
35	17.8	15.6	2.20	18.0	17			
40	15.6	13.6	1.93	15.9	15			
50	12.4	10.9	1.54	12.7	10			
60	10.4	9.09	1.28		8.0			
70	8.89	7.79	1.10					
80	7.78	6.81	0.96					
90	6.91	6.06	0.86		5.6			
100	6.22	5.45	0.77		5.2	6.7	11.8	
150	4.15	3.63	0.51					
200	3.11	2.73	0.39			4.0		

Values of Q are in units of 10^{-18} cm^2.
*Values are from model. See Table 5*b*.
†From *Cartwright et al.* [1977*b*] (who measured all v' in electron scattering experiment).
‡From *Finn and Doering* [1976] (who gave results for $v' = 0$ to 6 in an electron scattering experiment).
§From *Holland* [1969] (who measured $v' = 0$ to 6 in an optical emission experiment).
‖From *Chung and Lin* [1972] (who theoretically calculated all v').
¶From *Ajello* [1970 (who measured $v' = 0$ to 6 in an optical emission experiment).

TABLE 5*b*. Molecular Constants Used in Model

v'	C_{ij}	E_v (Rydberg)	$Q_{v'}$, 100 eV
0	2.213-2	0.6285	2.65
1	5.953-2	0.6436	7.12
2	8.824-2	0.6585	10.56
3	9.506-2	0.6731	11.38
4	8.334-2	0.6878	9.98
5	6.360-2	0.7016	7.61
6	4.352-4	0.7159	5.21
7	2.773-2	0.7297	3.32
8	1.667-2	0.7428	2.00
9	9.447-3	0.7557	1.13
10	5.215-3	0.7691	0.624
11	2.770-3	0.7816	0.315
12	1.472-3	0.7939	0.176
13	7.538-4	0.8065	0.092
14	3.736-4	0.8181	0.041

Here $\alpha = 7.1675$ for all v'. Molecular constants v', C_v, E_{ij}, and α (see equation (3)) are in atomic units, and $Q_{v'}$ (100 eV), which is based on (3) and (4), is in units of 10^{-19} cm^2 for each vibrational level (see text). Read 2.213-2 as 2.213×10^{-2}.

TABLE 6. Cross Section for N I (119.99 nm) Multiplet ($^4P \rightarrow {}^4S^0$)

	Relative Cross Section			Absolute Cross Section, 10^{-18} cm^2		
Energy	This Work	From *Mumma and Zipf* [1971*a*]	From *Aarts and de Heer* [1971]	This Work	From *Mumma and Zipf* [1971*a*]*	From *Aarts and de Heer* [1971]
20.10 (A.P)†	0					
22.5	0.09	0.0		0.40		
25	0.18	0.08		0.82	0.37	
27.5	0.26	0.15		1.18	0.69	
30	0.28	0.20		1.26	0.95	
32.5	0.30	0.25		1.36	1.19	
35	0.31	0.27		1.41	1.28	
37.5	0.33	0.29		1.50	1.37	
40	0.38	0.30		1.73	1.40	
45	0.52	0.41		2.35	1.93	
50	0.65	0.55		2.45	2.56	5.06
60	0.81	0.79		3.66	3.68	5.06
70	0.98	0.94		4.44	4.41	
80	0.99	0.99	1.03	4.48	4.66	4.86
90	1.00	1.00		4.52	4.69	
100	0.99	0.99	1.00	4.48	4.66	4.72
125	0.94	0.89		4.25	4.38	
150	0.89	0.87	0.86	4.04	4.08	4.07
200	0.77	0.76	0.74	3.48	3.55	3.47
250	0.70	0.66		3.17	3.08	
300	0.63	0.59	0.59	2.86	2.77	2.78
350	0.59	0.53		2.67	2.48	
400	0.55		0.47	2.48		2.20

*Cross section values multiplied by 0.693 correction factor at 100 eV [*Shemansky et al.*, 1985*a*].
†A.P. is appearance potential.

energies below 18 eV the vibrational cross-section curves of the $v' = 5$ and 1 levels intersect, and below 11 eV the $v' = 0$ and 5 levels intersect and change position in order of relative strength. These changing relative cross sections are reflected in the spectra of Figure 5 at 11 and 15 eV which show increasing relative band intensities originating from low v' of the $a^1\Pi_g$ state.

Thus the model and data in Figures 5 and 9 show that for low energies ($\varepsilon < 20$ eV) the vibrational cross sections deviate significantly from the Franck-Condon factor distribution and the band intensities are not in the ratio of the emission fractions given in Table 1.

A plot of the relative vibrational cross sections normalized to $v' = 0$ as a function of vibrational quantum number for several energies is shown in Figure 11. Both experimental data and model calculations for each vibrational level are shown for 11- and 15-eV energies. Marked differences of greater than 5% between the Franck-Condon distribution of relative vibrational cross sections and actual rates begin at $\varepsilon \sim 20$ eV and increase geometrically for each vibrational level

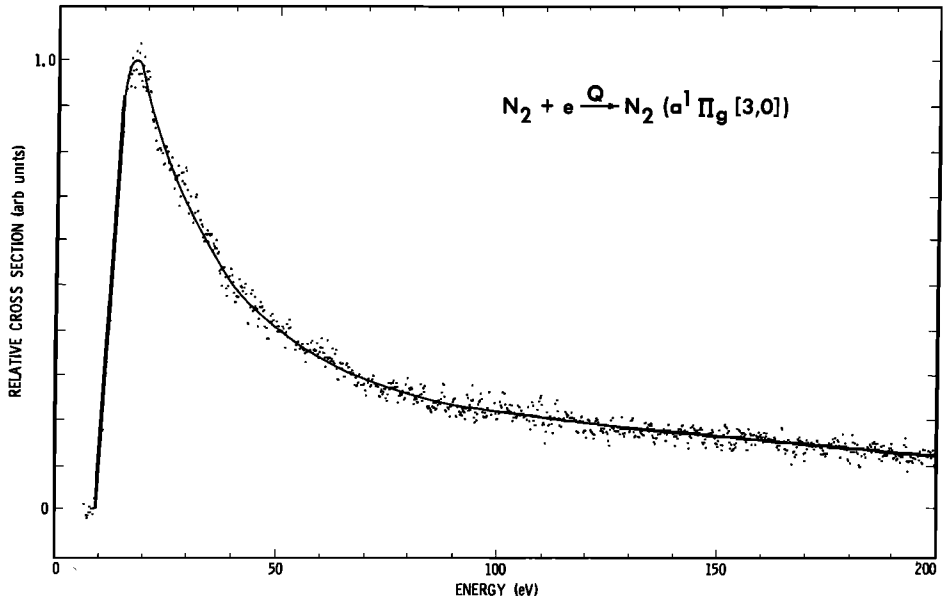

Fig. 6. Relative emission cross section of the $a^1\Pi_g$ (3, 0) vibrational band feature 11 at 135.4 nm from threshold to 200 eV with instrument band pass set to 1.2 nm. The data points are separated by 0.1955 eV.

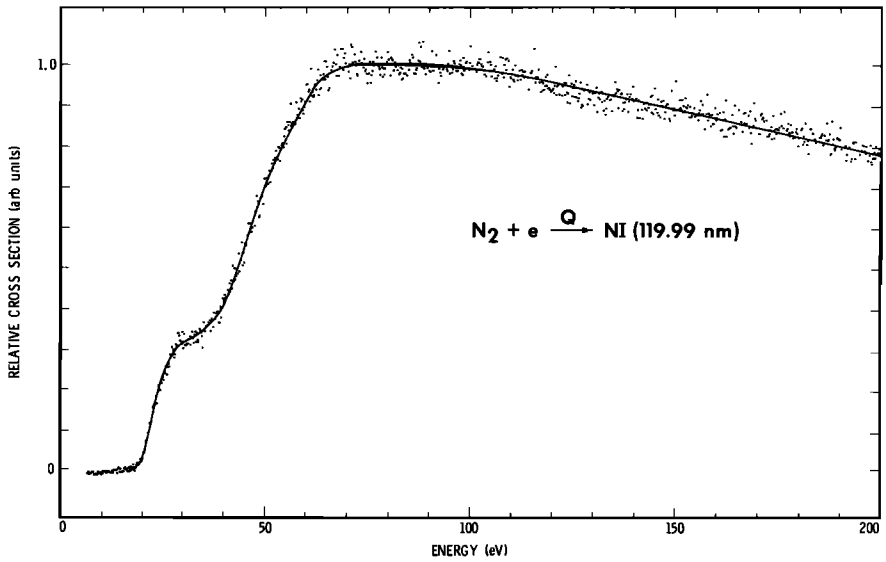

Fig. 7. Relative emission cross sections of the N I (119.99 nm) multiplet ($^4P \rightarrow {}^4S^0$) from threshold to 200 eV.

with each 2-eV decrease in energy. The experimental data and model are in near exact agreement at 11 and 15 eV except for $v' = 6$. A small amount of predissociation may occur at $v' = 6$. This result confirms the model calculation and the assertion that excitation shape functions are independent of vibrational level.

The experimental data points in Figure 11 are taken from analysis of 10 bands in Figure 5 as listed in Table 7. Table 7 lists the following information: (1) the measured energy dependence of the relative vibrational cross sections normalized to unity for the $v' = 0$ level and (2) the ratio of the low- and high-energy emission cross sections. The largest vibrational cross-section threshold effect that we observe is for the $v' = 6$ level. Figure 11 indicates that the vibrational cross-section ratio of $v' = 6$ to $v' = 0$ has decreased by a factor of ~5 in going from the high-energy distribution of vibrational cross sections ($\varepsilon > 20$ eV) to the experimentally measured set at 11 eV.

At energies above 20 eV, LBH features blended with N I multiplets, causing apparent departures from the Franck-Condon distribution. For example, features 7, 9, 15, 20, and 35 contain spectral contributions from both LBH vibrational features and N I multiplets. Figure 5 with spectra at 11 and 15 eV is important for unequivocal identification of LBH spectral contributions because these spectra contain uncontaminated LBH features. Thus the absence of features below 126 nm in the low-energy spectra of Figure 5 shows that most of the contribution to the spectral features below 126 nm for energies above 20 eV is from N I multiplets, e.g., feature 2. A discussion of the features below 120 nm will be delayed

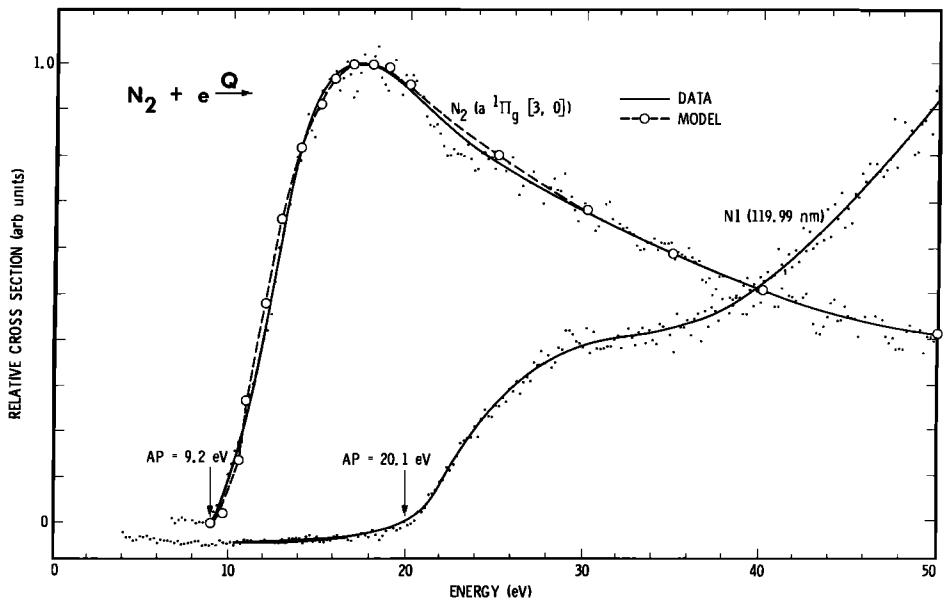

Fig. 8. Expanded energy scale of the cross-section data shown in Figures 6 and 7. The theoretical appearance potentials for the $a^1\Pi_g$ (3, 0) vibrational band and the 119.99-nm N I multiplet are shown. The experimental threshold appears at the theoretical appearance potential. The model of the (3, 0) band is plotted as a dashed line, and the average experimental curve is shown as a solid line.

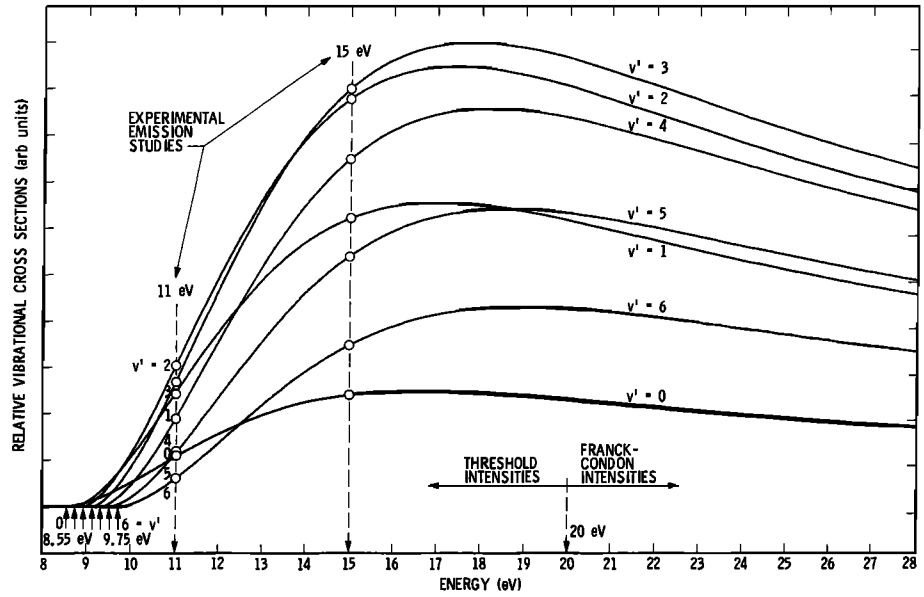

Fig. 9. Relative emission cross section of each vibrational level in the threshold region based. The cross-section curves are based on our modeled energy dependence given by equation (3) and constants given in Table 5. The open circles at 11 and 15 eV were used to construct the modeled points for 11 and 15 eV in Figure 11.

until a following paper is completed on band systems and N I multiplets in the EUV (40–120 nm).

Discussion

The results obtained here over an energy range from threshold to 200 eV consolidate many of the optical emission experiments, time of flight, and energy loss electron scattering results for the LBH bands obtained over more limited energy ranges. The importance of accounting for threshold effects in model calculations of N_2 $a^1\Pi_g$ state excitation has

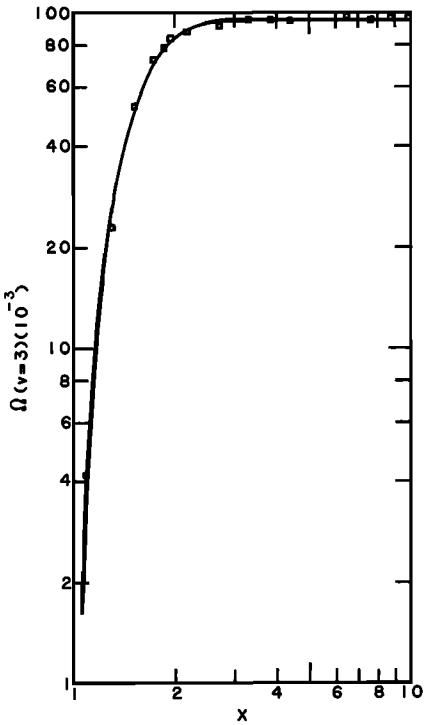

Fig. 10. Collision strengths of the (3, 0) band model and data. The model curve is based on (3) and constants in Table 5. Open squares represent experimental data points for the (3, 0) band.

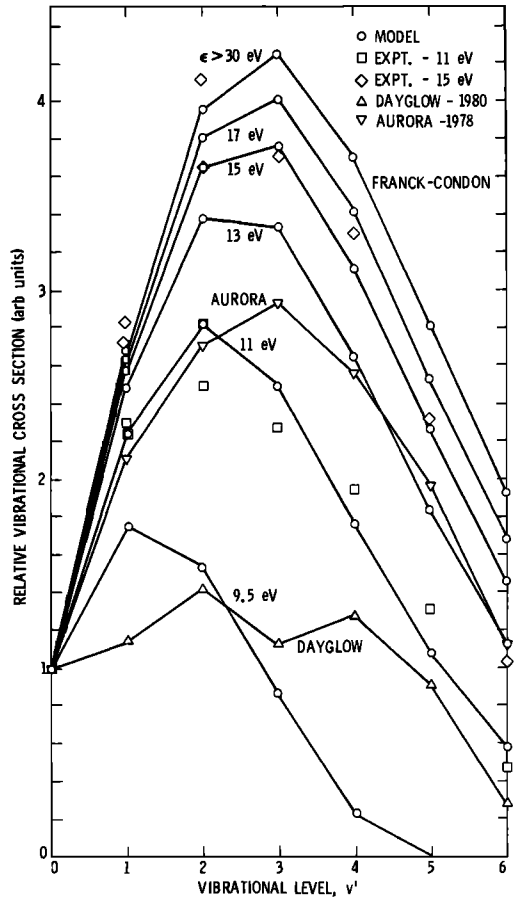

Fig. 11. Experimental data and model of the relative vibrational cross sections of the $a^1\Pi_g$ state normalized to unity for $v' = 0$ as a function of vibrational level for various energies. Recent dayglow and auroral are shown [*Meier et al.*, 1985]. The curves are based on (3) and (4) and constants in Table 5. Some vibrational levels show more than one experimental data point for cases where more than one band went into the analysis (see Table 7).

TABLE 7. Relative Vibrational Cross Sections as a Function of Electron Energy

Feature	Wavelength	Strongest Vibrational Band of Feature	Experimental Ratio of Low- and High-Energy Relative Emission Cross Sections: 11 eV, High Energy	15 eV, High Energy	Experimental Relative Vibrational Cross Section ($a^1\Pi_g$ State) Normalized to 1.0 to $v' = 0$: 11 eV	15 eV	High Energy, $\varepsilon > 20$ eV
6	129.9	(5, 0)	0.88	0.94	1.30	2.30	2.82
7	131.2	(6, 1)	0.44	0.60	0.45	1.01	1.93
9	132.5	(4, 0)	0.99	1.02	1.93	3.30	3.71
11	135.4	(3, 0)	1.00	1.00	2.27	3.70	4.25
13	138.4*	(2, 0)	1.20	1.08	2.49	3.71	3.96
16	143.0	(2, 1)	1.35	1.19	2.81	4.09	3.96
18	146.4	(1, 1)	1.61	1.14	2.28	2.76	2.68
24	155.4	(0, 2)	2.00	1.19	1.05	1.03	1.00
28	161.1	(0, 3)	1.78	1.09	0.94	0.95	1.00
33	168.7*	(1, 5)	1.59	1.22	2.25	2.85	2.68

*Contains 10% or greater contribution from weaker component within 2 Å of feature.

been demonstrated. In the low-energy energy range, excitation rates should be calculated for each vibrational level using accurate cross-section curves which include the exact threshold energy for each vibrational level. The threshold shift effect on excitation rates has not been generally recognized in the literature. The effect on the shape of the emission spectrum is quite dramatic in the low-energy region. This effect is expected to be especially important for other diatomic molecules, especially H_2, HD, D_2, CO, O_2, and other electron states of N_2 ($^1\Pi_u$, $^1\Sigma_u^+$, $^3\Pi_{u,g}$, $^3\Sigma_{u,g}^+$). The threshold effects on H_2, HD, and D_2 are pronounced, even for the allowed direct transitions like the Lyman and Werner systems. For example, the separation between $v' = 0$ and $v' = 15$ for the B state of the Lyman system is about 2 eV. Model calculations indicate threshold effects to the level of a few percent at energies beyond 50 eV.

Equation (3) can be averaged for an assumed thermal electron energy distribution using the exact integral equation,

$$\Omega_{ij}(Y) = C_{ij}\left[1 - 7!Y\left(\frac{(1+\alpha+Y)}{(\alpha+Y)^8} + \sum_{n=2}^{7}\frac{1}{n!(\alpha+Y)^{8-n}}\right)\right] \quad (5)$$

where $Y = E_{ij}/T_e$ and T_e is electron temperature in units of E_{ij}. The rate coefficient for excitation is then given by

$$k_{ij}(T_e) = 8.629 \times 10^{-6} T_e^{-1/2}[\Omega_{ij}(Y)/\omega_i] \cdot \exp(-Y) \quad \text{cm}^3\ \text{s}^{-1} \quad (6)$$

for T_e in Kelvin units.

Table 5 lists the values of the constant C_{ij} and E_{ij} for each of the $a^1\Pi_g$ vibrational levels. The application of (3) and (5) thus allows accurate model calculations of excitation rates at low electron energies, such as those encountered in earth aurorae and dayglow. The electron energy distribution in auroral and dayglow excitation is often conveniently approximated by a power law flux distribution, in which the differential electron flux is defined by the equation

$$\mathcal{F}_e\, d\varepsilon = \eta_0 \varepsilon^{-a}\, d\varepsilon \quad \text{el cm}^{-2}\ \text{s}^{-1} \quad (7)$$

where $\mathcal{F}_e$ is the differential number flux and η_0 and a are positive constants. The rate coefficients for excitation of the N_2 LBH upper state vibrational levels based on (7) are given by

$$k_{ij} = 4.686 \times 10^{13}\, C_{ij}\, E_{ij}^{-1/2}\, \frac{(a-1/2)}{a} \cdot \left\{1 - a\alpha^{(a-7)} \exp(\alpha)\,(6-a)! \cdot \left[1 - \frac{[(6-a), \alpha]!}{(6-a)!}\right]\right\} \quad \text{cm}^3\ \text{s}^{-1} \quad (8)$$

where E_{ij} is in Rydberg units. The only minor complication in the evaluation of (8) is the requirement for the calculation of the incomplete factorial function. The reader is reminded that the electron density involved in this rate calculation (equation (8)) refers only to that part of the population above the threshold energy E_{ij}. The excitation probability is then given by the product $[e]_{\text{eff}}k_{ij}$ (s^{-1}), where the effective electron density is

$$[e]_{\text{eff}} = 2.134 \times 10^{-14}\, \eta_0\, E_{ij}^{-(a-1/2)}\, \frac{1}{(a-1/2)} \quad \text{cm}^{-3} \quad (9)$$

Equations (8) and (9) must therefore always be applied in combination in a model calculation. If the electron temperature is low or the constant a is relatively large, substantial deviation in relative upper vibrational level excitation rates from a Franck-Condon factor distribution can be obtained because of differences in the threshold energies E_{ij}.

We list in Table 4 the relative cross section for excitation of the $a^1\Pi_g$ state found in this experiment and have compared results to other measurements. The excellent agreement between the various experiments is to be noted. Particularly good agreement to the 5% level occurs between the work of *Cartwright et al.* [1977*a*, *b*] and our results over most energies. Cartwright et al. measured the energy loss spectrum of the inelastically scattered electrons up to $v' = 10$ and thus measured the direct excitation cross section, including a predissociation contribution for $v' \geq 7$. Our work determined both the emission cross section (cascade plus direct cross sections) and the predissociation cross section. States which cascade to the a state are $b^1\Pi_u$, $b^1\Sigma_u^+$, $c_3^1\Pi_u$, and $c_4'^1\Sigma_u^+$ [*Huber and Herzberg*, 1979]. These transitions are allowed and have thresholds between 12 and 13 eV. The

excitation function of an electric dipole permitted transition differs from that for a magnetic dipole transition because the latter is excited mostly by electron exchange. At high energy ($\varepsilon > 300$ eV) an optically allowed transition has a cross-section dependence of $[\ln(\varepsilon)]/\varepsilon$, whereas the N_2 LBH transition has an asymptotic cross-section energy dependence of ε^{-1} above 20 eV, as shown in Figure 10. The close correspondence of the shape of the cross-section variation from the electron energy loss and electron-induced fluorescence experiments and the 5% agreement in the total electronic cross section suggests that the cascade cross section must be less than 5% of the total excitation cross section. The recent results of *Filippelli et al.* [1984] substantiate this result for the Gaydon-Herman singlet bands. They find that the $c_4'^1\Sigma_u^+ (v' = 0) \rightarrow a^1\Pi_g (v'')$ cascade contribution is 1×10^{-19} cm^2 near 80 eV. In Table 5 we compare our absolute values to other determinations of the $a^1\Pi_g$ absolute cross section. Some authors have measured the excitation cross section Q, and others have measured the emission cross section Q_E for $v' = 0$ to 6. The two cross sections are related by $Q_E = 0.877Q$ for $\varepsilon > 20$ eV. Excellent agreement certainly within the overlap of the allowable experimental errors (~25%) is found for the entire set of absolute cross sections over all energies. In particular, our values for the LBH cross section for this emission experiment agree to better than 5% with the value of the LBH cross section deduced from the *Cartwright et al.* [1977*a*, *b*] electron scattering energy loss experiment (Table 5, sixth column). We measure a peak LBH cross-section value that is within 25% of the earlier published value [*Ajello*, 1970]. The earlier *Ajello* [1970] cross section does not depend on the dissociative H Ly α cross section. The energy dependence has been corrected over that given in the earlier publication.

The $a^1\Pi_g$ state is 100% predissociated for $v' \geq 7$; there are no bands detected in the spectra originating at $v' = 7$, 8, and 9. For example, the (9, 0), (8, 0), (7, 0), and (8, 1) bands at 120.53, 122.66, 124.93, and 126.29 nm, respectively, are missing in the 11- and 15-eV spectra shown in Figure 5. The absence of these features in the spectra obtained at higher energies would be more difficult to discern owing to the blending of the N I lines and Birge-Hopfield bands with the candidate $v' \geq 7$ LBH bands. Thus the emission yield for $v' \geq 7$ is 0% at pressures where collisional suppression of breaking off of bands is not important [*Herman*, 1945; *Herzberg*, 1950]. This result for emission yield establishes an upper limit on the predissociation lifetime of 10^{-7} s. On the other hand the sharp absorption features for $v' \geq 7$ observed by *Vanderslice et al.* [1965] and the sharp energy loss spectra for $v' \geq 7$ by *Cartwright et al.* [1977*a*, *b*] put a lower limit of about 10^{-12} s on the predissociation lifetime. Thus $10^{-7} < \tau_0 < 10^{-12}$ where τ_0 is the predissociation lifetime.

In Table 6 we show the relative and absolute cross sections of the important resonance transition of N I at 119.99 nm. There is excellent agreement among the various experimenters as to its relative energy dependence. In addition a correction to the *Mumma and Zipf* [1971*a*] result with our revised calibration standard for H_2 [*Shemansky et al.*, 1985*a*, *b*] brings the two results into 5% agreement over energies greater than 30 eV, as Table 6 shows. The agreement with *Aarts and de Heer* [1971] is also about 5%. Thus our revised calibration standard for H_2 enables the N I (119.99 nm) emission multiplet cross section to be well established by these three experiments. The N I (119.99 nm) multiplet can serve as a calibration standard at 100 eV and 200 eV with average values of 4.67×10^{-18} cm^2 and 3.50×10^{-18} cm^2, respectively. Our measured values lie within 5% of the experimentally averaged values. The observed thresholds and comparisons to the relevant ionization and ionization excitation processes have been discussed before [*Ajello*, 1970; *Mumma and Zipf*, 1971*a*; *Aarts and de Heer*, 1971]. These same earlier publications indicate that the other strong multiplets in the FUV have the same energy dependence to about 10%. Thus we used the energy dependence of the 119.9-nm N I transition to give the set of 200-eV cross sections for the N I multiplets listed in Table 2.

The results obtained here should be particularly useful for model calculations of atmospheric phenomena in nitrogen systems. We have determined that the N_2 LBH system, which apparently is an important component in the understanding of energy deposition and atmospheric physical chemistry [*Meier et al.*, 1985], has a particularly simple excitation function. An accurate analytic fit to the cross section allows direct calculation of excitation effects over all energies above threshold. As we have pointed out above, threshold effects may have some importance in the understanding of some emission phenomena. Low-energy electrons play a strong role in auroral and dayglow activity [*Cartwright*, 1978; *Doering et al.*, 1975]. A recent analysis of the N_2 LBH system in dayglow and auroral observations by *Meier et al.* [1985] suggest that threshold effects may play a role in understanding the processes, but it is apparent that other unexplained complications are present [*Meier et al.*, 1985]. Figure 11 shows plots of the $a^1\Pi_g$ state vibrational excitation rates measured in 1978 and 1980 [see *Meier et al.*, 1985]. The 1978 non-Franck-Condon auroral vibrational population observed and modeled by *Meier et al.* [1985] can be explained by the threshold effect. However, the 1980 dayglow results, in particular, deviate substantially from expectations based on a simple photoelectron deposition model. Our calculations using mean measured photodetection energy spectra suggest that the typical dayglow distribution should approximately match the 17-eV case shown in Figure 11.

Acknowledgments. We thank A. Christensen and R. Meier for making the dayglow data of the LBH band system available prior to publication. We have benefited from discussions with S. Trajmar. The research described in this paper was carried out by the University of Southern California, the University of Arizona, and the Jet Propulsion Laboratory, California Institute of Technology, and was supported by the Air Force Office of Scientific Research and the National Aeronautics and Space Administration.

The Editor thanks R. R. Conway and another referee for their assistance in evaluating this paper.

REFERENCES

Aarts, J. F. M., and F. J. de Heer, Emission cross sections for NI and NII multiplets and some molecular bands for electron impact on N_2, *Physica*, *52*, 45, 1971.

Ajello, J. M., Emission cross sections of N_2 in the vacuum ultraviolet by electron impact, *J. Chem. Phys.*, *53*, 1156, 1970.

Ajello, J. M., The EUV spectrum of H_2O by electron impact, *Geophys. Res. Lett.*, *11*, 1195, 1984.

Ajello, J. M., and B. Franklin, Extreme ultraviolet studies of O_2 by electron impact, *J. Chem. Phys.*, *82*, 2519, 1985.

Ajello, J. M., and S. K. Srivastava, UV studies of electron impact excitation of CS_2, *J. Chem. Phys.*, *75*, 4454, 1981.

Ajello, J. M., S. K. Srivastava, and Y. L. Yung, Laboratory studies of UV emissions of H_2 by electron impact: The Werner and Lyman band systems, *Phys. Rev. A*, *25*, 2485, 1982.

Ajello, J. M., D. E. Shemansky, Y. L. Yung, and D. Kwok, Studies of extreme ultraviolet emission from Rydberg series of H_2 by electron impact, *Phys. Rev. A*, *29*, 636, 1984.

Borst, W. L., Excitation of several important metastable states of N_2 by electron impact, *Phys. Rev. A*, *5*, 648, 1972.

Cartwright, D. C., Vibrational population of the excited states of N_2 under auroral conditions, *J. Geophys. Res.*, *83*, 517, 1978.

Cartwright, D. A., A. Chutjian, S. Trajmar, and W. Williams, Electron impact excitation of the electronic states of N_2, I, Differential cross sections at incident energies from 10 to 50 eV, *Phys. Rev. A*, *16*, 1013, 1977*a*.

Cartwright, D. C., S. Trajmar, A. Chutjian, and W. Williams, Electron impact excitation of the electronic states of N_2, II, Integral cross sections at incident energies from 10 to 50 eV, *Phys. Rev. A*, *16*, 1041, 1977*b*.

Chung, S., and C. C. Lin, Excitation of the electronic states of the nitrogen molecule by electron impact, *Phys. Rev. A*, *6*, 988, 1972.

Doering, J. P., W. K. Peterson, C. O. Bostrom, and J. C. Armstrong, Measurement of low-energy electrons in the day airglow and dayside auroral zone from Atmosphere Explorer C, *J. Geophys. Res.*, *80*, 3934, 1975.

Filippelli, A. R., S. Chung, and C. C. Lin, Electron-impact excitation of the $D^3\Sigma_u^+$ and $c_4'^1\Sigma_u^+$ Rydberg states of N_2, *Phys. Rev. A*, *29*, 1709, 1984.

Finn, T. G., and J. P. Doering, Measurement of the 13 to 100 eV electron impact excitation cross section for the $X^1\Sigma_g^+ \rightarrow a^1\Pi_g$ transition in N_2, *J. Chem. Phys.*, *11*, 4490, 1976.

Gentieu, E. P., P. D. Feldman, and R. R. Meier, Spectroscopy of the extreme ultraviolet dayglow at 6.5Å resolution: Atomic and ionic emissions between 530 and 1240Å, *Geophys. Res. Lett.*, *6*, 325, 1979.

Herman, R., Contribution to the study of the spectra of nitrogen, *Ann. Phys. Paris*, *20* (11), 241, 1945.

Herzberg, G., *Spectra of Diatomic Molecules*, p. 433, Van Nostrand, New York, 1950.

Holland, R. F., Excitation of nitrogen by electrons: The Lyman-Birge-Hopfield system of N_2, *J. Chem. Phys.*, *51*, 3940, 1969.

Huber, K. P., and G. Herzberg, *Molecular Spectra and Molecular Structure*, vol. IV, *Constants of Diatomic Molecules*, p. 240, Van Nostrand, New York, 1979.

Huffman, R. E., F. J. LeBlanc, J. C. Larrabee, and D. E. Paulsen, Satellite vacuum ultraviolet airglow and auroral observations, *J. Geophys. Res.*, *85*, 2201, 1980.

Kelly, R. L., and L. J. Palumbo, Atomic and ionic emission lines below 2000 angstroms: Hydrogen through krypton, *Rep. 7599*, Nav. Res. Lab., Washington, D. C., 1973.

Lofthus, A., and P. H. Krupenie, The spectrum of molecular nitrogen, *J. Chem. Ref. Data*, *6*, 113, 1977.

Meier, R. R., D. J. Strickland, P. D. Feldman, and E. P. Gentieu, The ultraviolet dayglow, 1, Far UV emissions of N and N_2, *J. Geophys. Res.*, *85*, 2177, 1980.

Meier, R. R., R. R. Conway, D. E. Anderson, Jr., P. D. Feldman, R. W. Eastes, E. P. Gentieu, and A. B. Christensen, The ultraviolet dayglow at solar maximum, 3, Photoelectron-excited emissions of N_2 and O, *J. Geophys. Res.*, *90*, 6608, 1985.

Morgan, H. D., and J. E. Mentall, EUV studies of N_2 and O_2 produced by low energy electron impact, *J. Chem. Phys.*, *78*, 1747, 1983.

Mumma, M. J., Molecular branching-ratio method for intensity calibration of optical systems in the vacuum ultraviolet, *J. Opt. Soc. Am.*, *62*, 1459, 1972.

Mumma, M. J., and E. C. Zipf, Dissociative excitation of vacuum-ultraviolet emission features by electron impact on molecular gases, II, N_2, *J. Chem. Phys.*, *55*, 5582, 1971*a*.

Mumma, M. J., and E. C. Zipf, Calibration of vacuum-ultraviolet monochromators by the molecular branching-ratio technique, *J. Opt. Soc. Am.*, *61*, 83, 1971*b*.

Mumma, M. J., and E. C. Zipf, Dissociative excitation of vacuum ultraviolet emission features by electron impact on molecular gases, I, H_2, and O_2, *J. Chem. Phys.*, *55*, 1661, 1971*c*.

Paresce, F., M. Lampton, and J. Holberg, Extreme ultraviolet emissions from an aurora, *J. Geophys. Res.*, *77*, 4773, 1972.

Park, H., P. D. Feldman, and W. G. Fastie, The extreme ultraviolet (750–1230 A) spectrum of an aurora, *Geophys. Res. Lett.*, *4*, 41, 1977.

Pilling, M. J., A. M. Bass, and W. Braun, A curve of growth determination of the *f*-values for the fourth positive system of CO and the Lyman-Birge-Hopfield system of N_2, *J. Quant. Spectrosc. Radiat. Transfer*, *11*, 1593, 1971.

Rottman, G. J., P. D. Feldman, and H. W. Moos, Far ultraviolet spectra and altitude profiles of the dawn airglow, *J. Geophys. Res.*, *78*, 258, 1973.

Shemansky, D. E., N_2 Lyman-Birge-Hopfield system, *J. Chem. Phys.*, *51*, 5487, 1969.

Shemansky, D. E., and J. M. Ajello, The Saturn spectrum in the EUV-electron excited hydrogen, *J. Geophys. Res.*, *88*, 459, 1983.

Shemansky, D. E., J. M. Ajello, and D. T. Hall, Electron excitation of H_2: Rydberg band systems and the benchmark dissociative cross section of H Lyman-α, *Astrophys. J.*, *296*, 765, 1985*a*.

Shemansky, D. E., J. M. Ajello, D. T. Hall, and B. Franklin, Vacuum ultraviolet studies of electron impact excitation of He: Excitation of He(n^1P^0) Rydberg series and ionization excitation of He^+ (nl) Rydberg series, *Astrophys. J.*, *296*, 774, 1985*b*.

Srivastava, S. K., A. Chutjian, and S. Trajmar, Absolute elastic differential electron scattering cross sections in the intermediate energy region, I, H_2, *J. Chem. Phys.*, *63*, 2659, 1975.

Strobel, D. F., and D. E. Shemansky, EUV emission from Titan's upper atmosphere: Voyage 1 encounter, *J. Geophys. Res.*, *87*, 1361, 1982.

Takacs, P. Z., and P. D. Feldman, Far ultraviolet atomic and molecular nitrogen emissions in the dayglow, *J. Geophys. Res.*, *82*, 5011, 1977.

Trajmar, S., and D. F. Register, Experimental techniques for cross section measurements, in *Electron Molecule Collisions*, edited by K. Takayanagi and I. Shimamura, Plenum, New York, 1984.

Vanderslice, J. T., S. G. Tilford, and P. G. Wilkinson, The high-resolution absorption spectrum of nitrogen from 1060 to 1520 Å, I, The $a^1\Pi_g \rightarrow X^1\Sigma_g^+$ system, *Astrophys. J.*, *141*, 395, 1965.

Wiese, W. L., M. W. Smith, and B. M. Glennon, *Atomic Transition Probabilities*, vol. 1, *Hydrogen Through Neon*, *Natl. Stand. Ref. Data Ser.*, vol. NSRDS-NBS4, U.S. National Bureau of Standards, Washington, D. C., 1966.

Zipf, E. C., and R. W. McLaughlin, On the dissociation of nitrogen by electron impact and by EUV photo-absorption, *Planet. Space Sci.*, *26*, 449, 1978.

J. M. Ajello, Jet Propulsion Laboratory, 4800 Oak Grove Drive, Pasadena, CA 91109.

D. E. Shemansky, Lunar and Planetary Laboratory, University of Arizona, Tucson, AZ 85713.

(Received January 4, 1985;
revised May 13, 1985;
accepted May 24, 1985.)